3.3.4 Sensitivity Analysis

A sensitivity analysis was performed in order to determine the relative influence of different input parameters on the flow model. Seven different scenarios were tested (Table 6), which include varying the hydraulic conductivity of the fractured bedrock (scenarios 1-3), varying the hydraulic conductivity of the surficial deposits (4-5), and varying the imposed recharge (6-7).

Table 6 Description of sensitivity analysis scenarios. Each case refers to changes with respect to the base case (calibrated) model.

Scenario	Description	Figures (found in Annex B)
1	Hydraulic conductivities of the bedrock × 10	B1.B, B2.B, B3.B, B4.B, B5.B
2	Hydraulic conductivities of the bedrock ×0.1	B1.C, B2.C, B3.C, B4.C, B5.C
3	Hydraulic conductivities of the bedrock ×0.01	B1.D, B2.D, B3.D, B4.D, B5.D
4	Hydraulic conductivities of the surficial deposits ×10	B1.E, B2.E, B3.E, B4.E, B5.E
5	Hydraulic conductivities of the surficial deposits ×0.1	B1.F, B2.F, B3.F, B4.F, B5.F
6	Imposed recharge ×10	B1.G, B2.G, B3.G, B4.G, B5.G
7	Imposed recharge ×0.1	B1.H, B2.H, B3.H, B4.H, B5.H

The sensitivity analysis (Annex B) shows that the model is relatively insensitive to variations in the surficial deposit hydraulic conductivity (Figures B1.A, B1.E, and B1.F). While the depth of active flow in the St. Lawrence Lowlands is only slightly sensitive to variations in the imposed recharge and bedrock hydraulic conductivity, in the Appalachian Highlands, the depth of active flow seems to be very sensitive to the increase in hydraulic conductivity of the bedrock and to fluctuations in the recharge value (Figures B1.A, B1.B, B1.C, B1.D, B1.G and B1.H).

The sensitivity analysis also confirms that deep intermediate flow and regional flux is highly affected by the bedrock hydraulic conductivity and to a lesser degree by the imposed recharge (Figures B1.A, B1.B, B1.C, B1.D, B1.G and B1.H).

3.4 Groundwater Age Simulations

In addition to using groundwater flownets, simulated mean groundwater ages can also be useful for interpreting flow systems. Groundwater age is defined as the time elapsed since water entered the groundwater system (Kazemi et al. 2006; Goode 1996). In the simplest form of this definition, the kinetic or advective age of groundwater can be simulated by tracking particles along the groundwater flow lines. The time taken by individual particles to travel across the system from recharge to discharge would then yield groundwater ages. This method, also known as the piston flow model, is based on the velocity field derived from a groundwater flow model and assumes that a groundwater molecule (or a conservative tracer) migrates along flow paths without mixing (Goode 1990; Kazemi et al. 2006; Bethke and Johnson 2008).

Although groundwater flow systems are defined by streamlines or flow paths, individual water molecules entering the subsurface will mix and disperse along and across these flow paths, each following a unique pathway (Bethke and Johnson 2008). A more realistic definition of groundwater age would then be the average time that a group of water molecules of a given sample has spent in the subsurface (Bethke and Johnson 2008). This definition also better reflects the analytical methods used to measure groundwater ages of a given water sample using age tracers; it is not the specific age of individual molecules that is measured but rather the concentration ratios of various molecule groups which yield an average age.

In the TR2 groundwater model, mean groundwater age is taken to be the average (mean) age of a packet of water molecules at a given point in space (x,y) (Molson & Frind, 2017), and is calculated using Goode's (1996) method for direct simulation of groundwater age. The method uses an analogy to solute transport in which the concentration (kg/m^3) is replaced by the groundwater age. The age mass, the product of groundwater age, fluid density and sample volume can then be mixed, dispersed and transported as a solute using the advection-dispersion transport equation through a porous medium (Equation 11; see also (Molson & Frind, 2012):

$$\frac{\partial}{\partial x_i}\left(D_{i,j}\frac{\partial A}{\partial x_j}\right) - v\frac{\partial A}{\partial x_i} + 1 = 0 \quad (11)$$

where,

A= Mean age (T)
$D_{i,j}$ = Hydrodynamic dispersion tensor (L^2/T)
v= velocity (L/T)
+1 : Age growth factor (1 day/day)

TR2 is used herein to simulate advective-dispersive groundwater ages along the studied cross-Section. Comparisons are then made between these advective-dispersive ages, particle-track based advective ages, and later with measured ^{14}C ages.

3.4.1 Advective-Dispersive Groundwater Age

The calibrated steady-state groundwater flow model presented in Section 3.3 was used as the base velocity field to simulate mean groundwater ages within the 2D cross-Section of the Chaudière-Appalaches regional model. A finite element mesh identical to the flow model was used in the age transport model.

3.4.1.1 Transport Model Boundary Conditions and Parameters

In the age transport model, lateral and bottom boundaries are set as zero age-mass gradient Type-2 (Neumann) boundaries. Those Sections of the top surface water table which act as inflow recharge boundaries are set as a Type-1 (Dirichlet) boundary condition with a fixed age of A=0 days. Surface nodes acting as discharge points, that is nodes connected to elements with an outward pointing velocity vector, are applied a zero-gradient age boundary condition. A growth rate of +1 day/day ensures the aging of water as the simulation progresses over time until steady-state was reached between the constant ageing of water and rejuvenation from younger recharge water.

The dispersion tensor D_{ij} in Equation 11 is defined using the Lichtner dispersion formulation (Lichtner et al. 2002) which has four dispersivity components: two longitudinal (α_{LH} and α_{LV}) and two transverse dispersivities (α_{TH} and α_{TV}). The angle between the velocity vector and the vertical axis is used to determine the dispersion terms in the tensor. To define the longitudinal horizontal dispersity (α_{LH}), Xu and Eckstein (1995) provide a

relationship between dispersivity and the field scale which was derived from a weighted statistical method giving less importance to less reliable data. With their method, the increase in longitudinal dispersivity with scale is considerably reduced when the flow spatial scale exceeds 1 km, yielding more realistic dispersivities for large-scale studies such as that presented herein. Based on Xu and Eckstein (1995), the longitudinal horizontal dispersivity of the current transport model was set to 50 m, which is also consistent with the Schulze-Makuch (2005) set of porous media-specific equations for defining the relationship between scale and dispersivity. The longitudinal vertical dispersivity (α_{LV}) was set to 10 m, while the two transverse dispersivities were set to 0.05 m. The molecular diffusion coefficient was assumed 1×10^{-10} m^2/s, similar to a conservative tracer. Similar dispersion and diffusion terms were applied in 3D age transport modelling by Molson & Frind (2012).

The Peclet accuracy criterion, which constrains the spatial discretization depending on the relative magnitude of advection to dispersion (see Molson & Frind, 2017), is respected throughout most of the domain in the x direction, with about 90% of the elements respecting the criterion. However, due to the relatively low, but realistic, vertical dispersivity, about 54% of the elements respect the y-direction Peclet criterion. To reduce simulation times, time steps were increased progressively (Table 7) until steady-state was reached. The Courant stability criterion, which constrains the time step (Molson & Frind, 2017) is generally respected in both the x and y directions for all time steps (Table 7). Since the simulations showed good convergence and relatively minor numerical oscillations, the spatial and temporal discretization was considered acceptable.

Table 7 Time steps and stability criteria for the age transport model

From (day)	To (day)	Time step (days)	Time step (years)	Elements respecting the Courant criteria: x-direction (%)	Elements respecting the Courant criteria: y-direction (%)
0	$5x10^6$	100	0.27	99	96.4
$5x10^6$	$1x10^8$	1000	2.74	96.8	95.2
$1x10^8$	$1x10^9$	10000	27.38	94.3	92.9
$1x10^9$	$1x10^{10}$	50000	136.89	91.9	90.1
$1x10^{10}$	$2x10^{10}$	100000	273.76	90.7	88.5
$2x10^{10}$	$1x10^{11}$	1000000	2737.85	80.8	80.9

3.4.1.2 Mean Groundwater Age Distribution

The advective-dispersive groundwater age simulation reached steady state at 47.54 Ma for the base case scenario (Figures 29 to 34), which corresponds to the maximum simulated groundwater residence times in the Grenville basement rock. The nested flow systems identified in Section 3.3 create a unique mean age distribution which is organized into a complex pattern.

The active flow layer within the local flow system is characterised by short residence times, with mean groundwater ages being generally less than 100 years old (Figures 31 to 34). Interestingly, the mean age simulation shows that the depth of local flow systems extends well below the active flow layer. With mean ages exponentially increasing with depth, the maximum mean age of groundwater in the local flow systems is 100,000 years (Figures 31 to 34). The exponential increase in groundwater ages is attributed to the exponential decrease in the bedrock hydraulic conductivity.

Furthermore, while the presence of an intermediate flow system in the Appalachian Highlands was clear from the flow simulation, the direct simulation of mean groundwater ages also suggested the existence of such a system with a similar age distribution in the St. Lawrence Lowlands, between about 15,000 m and 30,000 m along the Section (Figures 29 and 34).

However, contrary to the Appalachian Highlands, in the St. Lawrence Lowlands the age distribution is marked by an abrupt transition between the regional and the smaller scale flow systems. In some portions of the cross-Section, for example, the mean age gradient spans two orders of magnitude over very short spatial scales on the order of 50 to 100 meters. This is consistent with Zijl's (1999) observation that in real steady-state flow systems, mixing zones between transport systems are relatively thin, and that the interface is generally sharp between water bodies with different water qualities (or ages) which belong to different flow systems.

On a regional scale, the average residence times in the deep flow system gradually increase toward the discharge area. Regional flow in the St. Lawrence Lowlands seems to follow a deep preferential pathway through the carbonate platform before emerging near the St.

Lawrence River. This is due to the difference in the assigned hydraulic conductivities between the Lorraine formation, the Carbonate platform and the Utica Shale. Among these three units, the Carbonate platform was assigned the highest hydraulic conductivity while the Utica shale was assigned the lowest, creating a hydraulically isolated permeable unit in which water could travel faster than in the overlying and underlying geologic units. Slower flow above the carbonate platform results in an inverted distribution of groundwater residence times where older groundwater in the shale can be found above younger water in the carbonates (Figure 29).

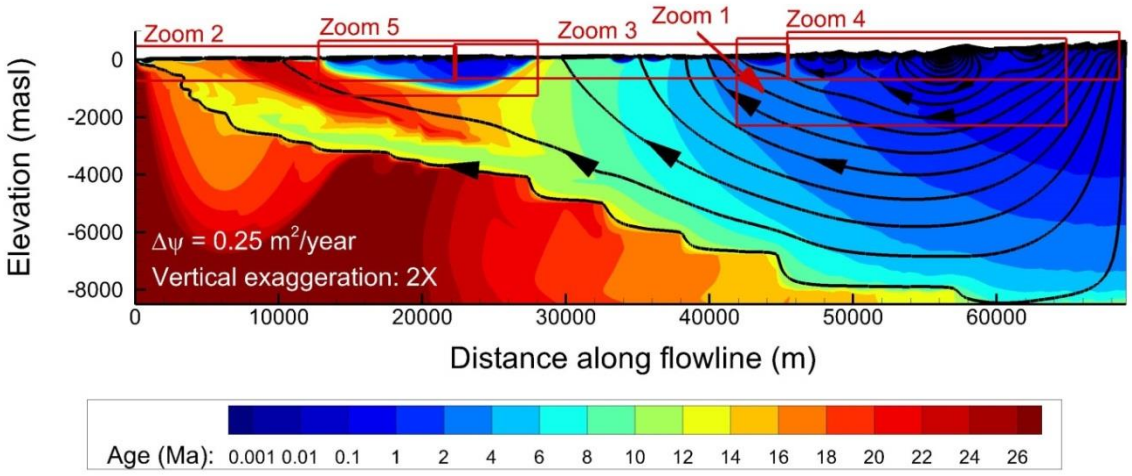

Figure 29 Simulated mean groundwater ages with superimposed streamlines from the calibrated flow model.

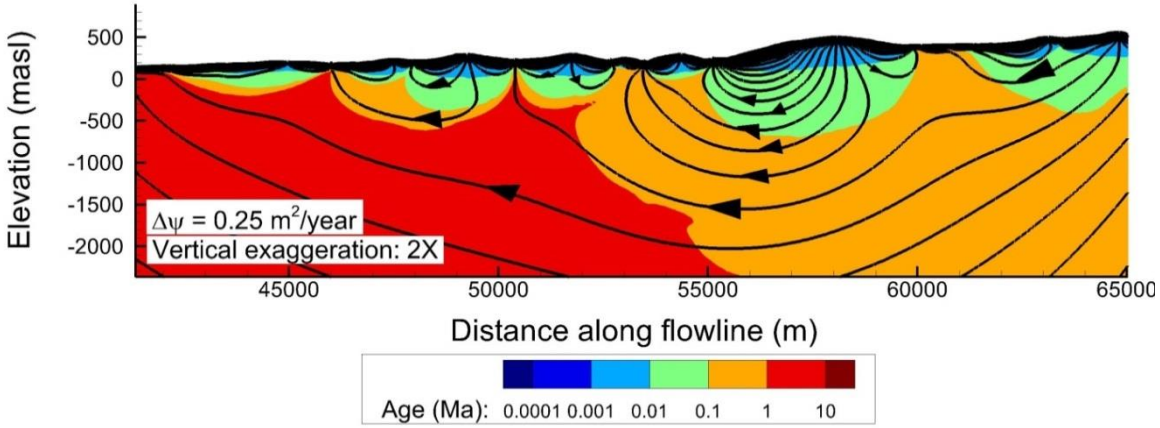

Figure 3029 Simulated mean groundwater ages with superimposed streamlines from the calibrated flow model Zoom 1 (Appalachian Highlands): mean age and streamlines (location shown in Fig. 30).

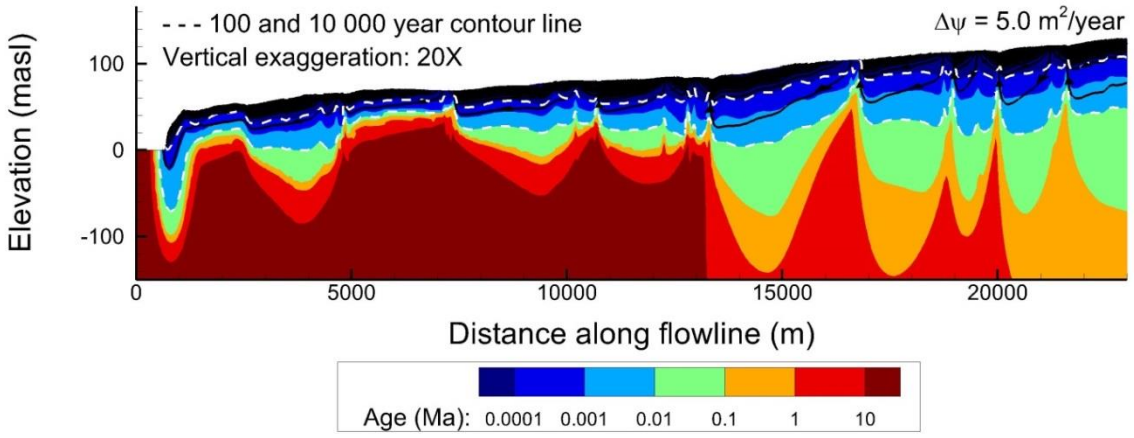

Figure 31 Simulated mean groundwater ages with superimposed streamlines from the calibrated flow model Zoom 2 (St. Lawrence Lowlands close to St. Lawrence River): mean age and streamlines (location shown in Fig. 30).

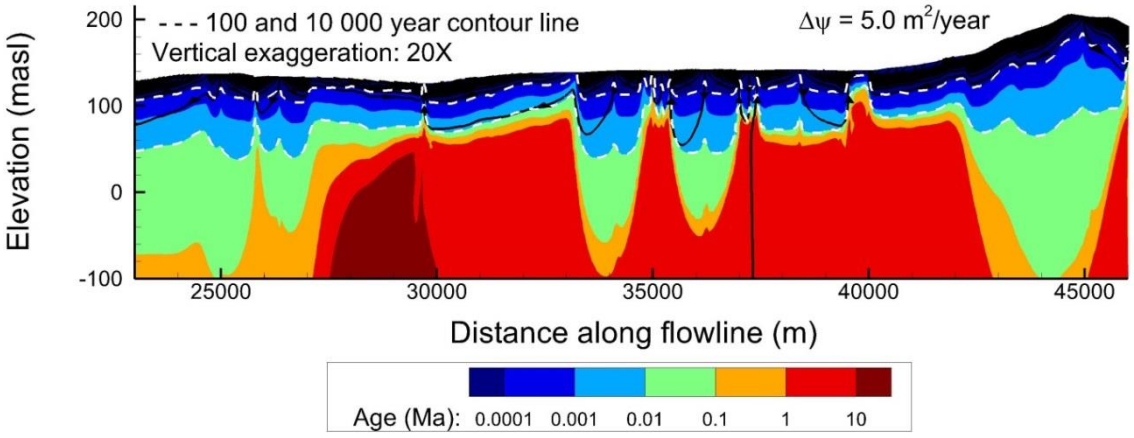

Figure 30 Simulated mean groundwater ages with superimposed streamlines from the calibrated flow model Zoom 3 (St. Lawrence Lowlands close to Appalachian front): mean age and streamlines (location shown in Fig. 30).

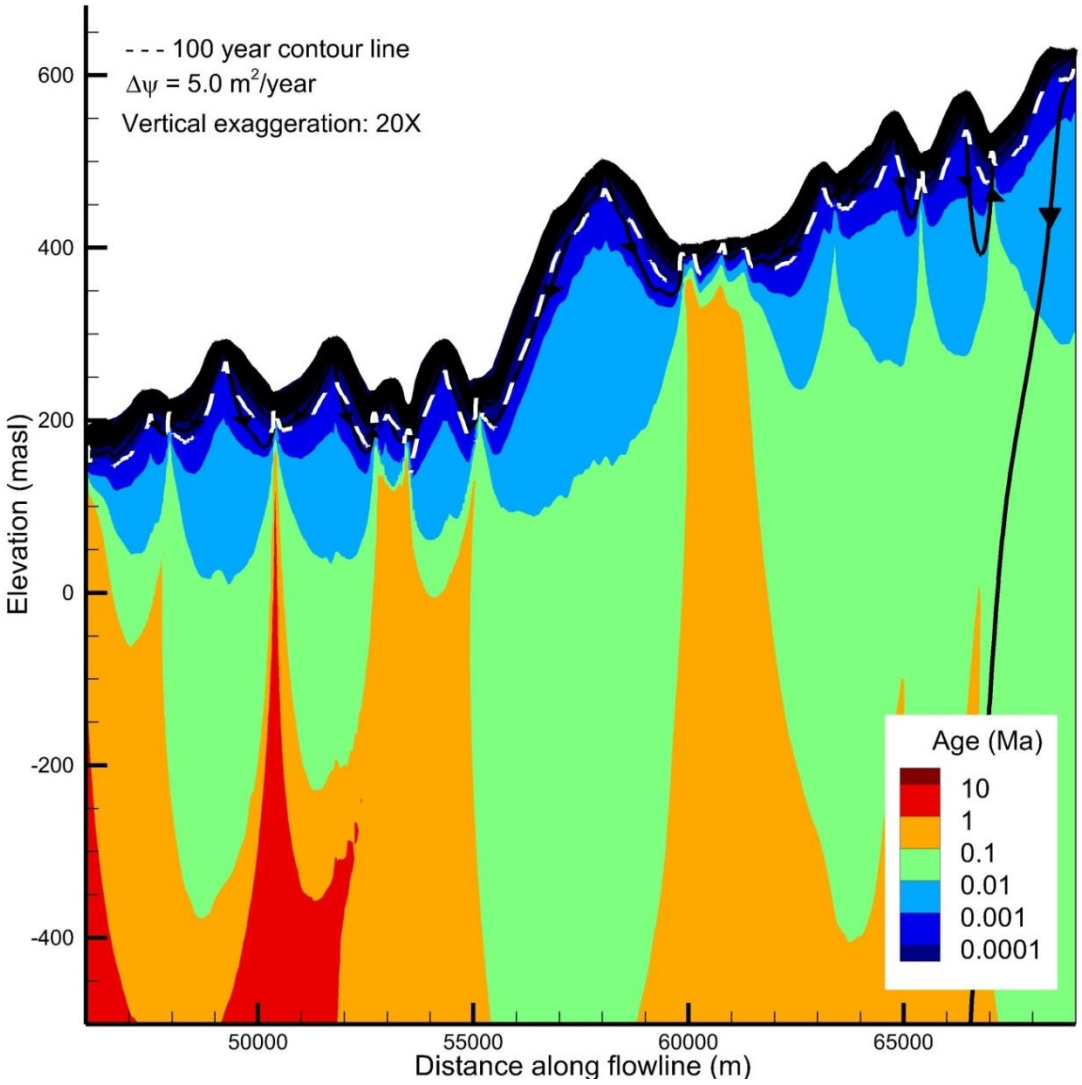

Figure 32 Simulated mean groundwater ages with superimposed streamlines from the calibrated flow model Zoom 4 (Appalachian Highlands): mean age and streamlines (location shown in Fig. 30).

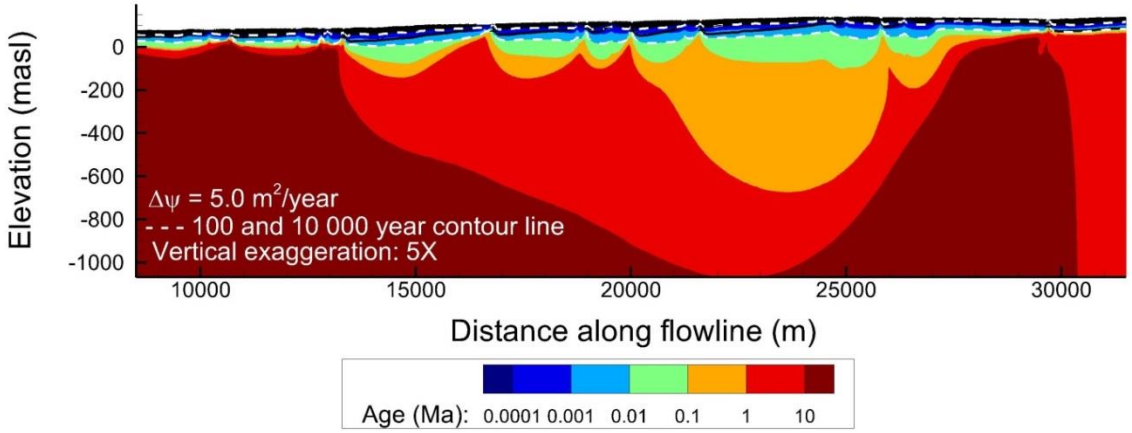

Figure 33 Simulated mean groundwater ages with superimposed streamlines from the calibrated flow model Zoom 5 (middle of St. Lawrence Lowlands): mean groundwater age and streamlines

3.4.2 Comparison between Advective and Advective-Dispersive Groundwater Ages

While the preceding mean age simulation fully accounts for age growth along flow lines as well as dispersive age mixing across flow lines, the approach is computationally demanding, requiring long simulation times because of the Courant constraint on the time steps. As an alternative, simulation of purely advective age growth along streamlines, but neglecting dispersive mixing, is much faster. In this Section, the two approaches are compared using the Chaudière-Appalaches cross-Section flow model.

Advective groundwater ages were here calculated using particle tracking with Tecplot (©Tecplot Inc. 2014), which tracks particles by integrating the velocity field using a 4th order Runge-Kutta method. The flow velocities were obtained from the simulated nodal streamfunctions, and are located at the centroids of the triangular elements (Molson & Frind, 2017). Particle tracks and corresponding advective ages are superimposed on the advective-dispersive age distribution in Figures 35 to 37.

For intermediate and regional flow paths, just below the local transport systems, total advective ages and advective-dispersive mean ages appear to be in the same order of magnitude. This is attributed to the relatively limited mixing between old and young waters along these deeper and longer flowpaths. At the discharge points, however, the total

advective ages are much greater than advective-dispersive mean ages since the latter are diluted by dispersion with younger waters of the local flow system.

Using particle tracking to define groundwater ages might thus be misleading since old advective age at the end of a single flow line coming from a deep flow system does not mix with younger, more rapidly flowing water. A tracked particle essentially represents very a small volume of water entering a discharge area where the influx of young water would be much greater. Advective travel times along regional flow paths are therefore not likely to be represented in mean groundwater ages of samples collected at the end of a flow path.

However, particle tracking also suggests that diffusion between regional and local flow systems must be significant. For example, in Figure 38, maximum advective ages in the local flow systems are less than 1 Ma, while the advective-dispersive mean groundwater ages are between 1 and 10 Ma. In other words, advective-dispersive groundwater ages at the base of local flow systems are much older than the advective travel times, as seen in the high vertical age gradient across the interface between the local and regional flow systems. Since regional flow paths circumvent the shallow local flow systems, exiting the system further downgradient, mean groundwater ages in the local flow systems are thus strongly affected by upward vertical diffusion of age mass from the slow moving regional systems. Transverse vertical hydrodynamic dispersion may also play a role.

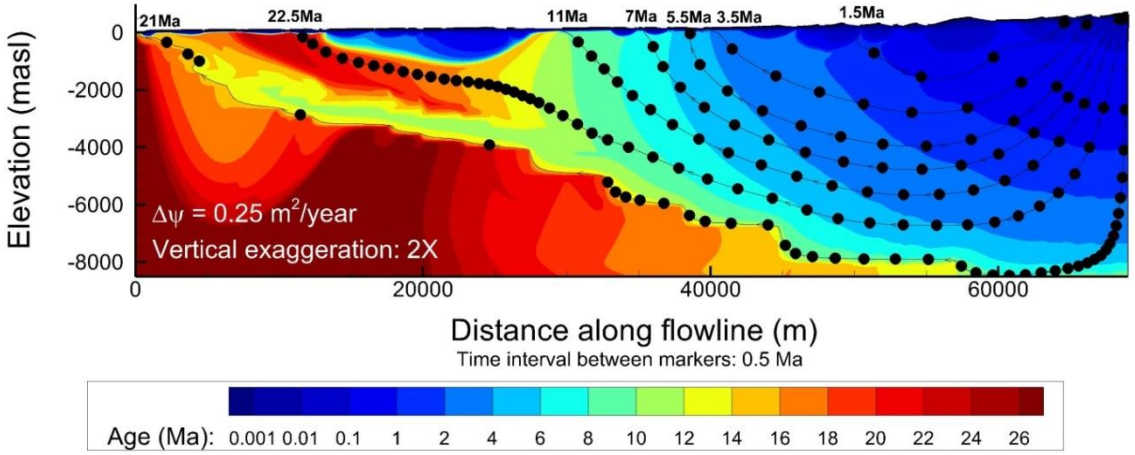

Figure 35 Calibrated flow model: mean age distribution and advective particle tracks. Times at top discharge points refer to final advective residence times between recharge and discharge points along selected streamlines.

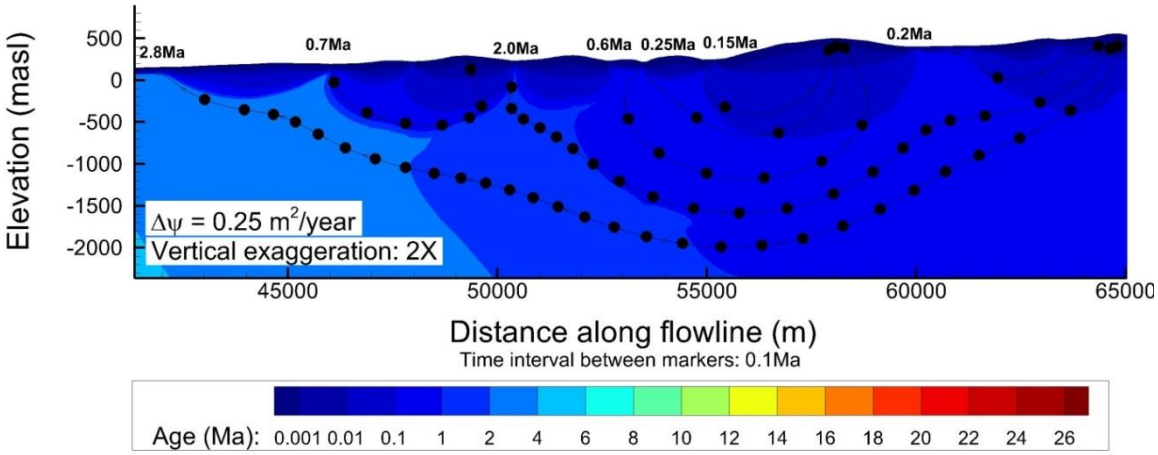

Figure 34 Calibrated flow model Zoom 1 (Appalachian Highlands): mean age distribution and advective particle tracks. Times at top discharge points refer to final advective residence times between recharge and discharge points along selected streamlines.

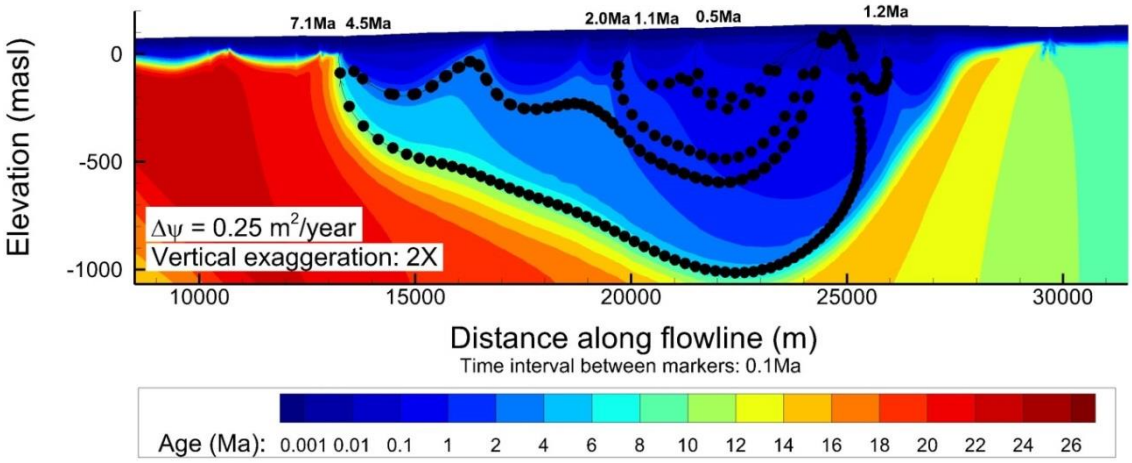

Figure 36 Calibrated flow model Zoom 5 (middle of St. Lawrence Lowlands): mean age distribution and advective particle tracks. Times at top discharge points refer to final advective residence times between recharge and discharge points along selected streamlines.

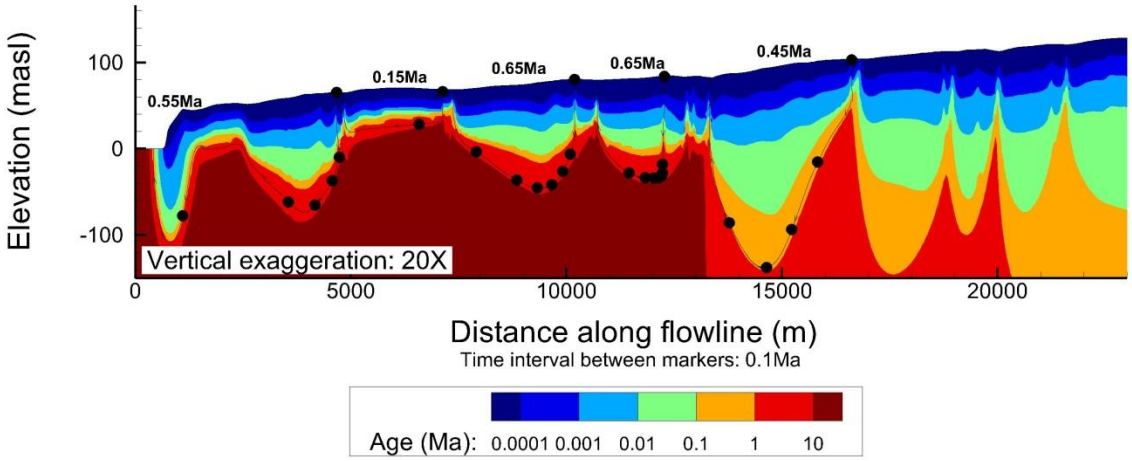

Figure 37 Calibrated flow model Zoom 2 (St. Lawrence Lowlands close to St. Lawrence River): mean age distribution and particle tracks (location shown in Fig. 30). Times at top discharge points refer to final advective residence times between recharge and discharge points along selected streamlines.

3.5 Parametric study on faults

The Utica Shale formation, located under the study area, was recently targeted by the oil and gas industry as an unconventional natural gas reservoir. However, public debate surrounding the environmental risks associated with such exploitation has raised many questions with respect to possible aquifer contamination (Rivard et al. 2014; Lavoie et al. 2014; Lefebvre 2017; CAA 2014).

While surface release of fluids related to unconventional oil and gas operations (Vengosh et al. 2014) and well integrity (Roy et al. 2016; Nowamooz et al. 2015) pose the greatest threat to aquifers, geochemical evidence also seems to point to instances in which deep seated fluids migrate to the surface along natural preferential flow pathways, such as faults (Révész et al. 2010; Warner et al. 2012). Yet, much debate still exists surrounding the possibility and the probability of shallow aquifer contamination through such pathways (Lefebvre 2017). While the question is often viewed from the perspective of the impact of fracking on fluid migration (Myers 2012; Gassiat et al. 2013; Flewelling and Sharma 2014; Birdsell et al. 2015; Lange et al. 2013; Kissinger et al. 2013), natural mechanisms, such as regional flow which can contribute to the upward migration of natural formation fluids prior to exploitation, is less often looked at.

Based on the observation of saline waters in valleys, Warner et al. (2012) hypothesised that the combination of high hydrodynamic pressure at depth under discharge areas (from regional flow, for instance) and the presence of higher permeability fracture zones can induce steep hydraulic gradients which could lead to migration of fluids between deeper strata and the surface. Indeed, this phenomenon seems to be occurring in our study area. Pinti et al. (2013) suggested, based on methane concentration observations, that the Yamaska Fault, an extension of the Jacques-Cartier River Fault (Figures 2 and 3) in our study area, could act as a connection between deep formations and surface aquifers. Moreover, focusing their research on the Lotbinère study area, located at the northern end of the modeled cross-Section (Figures 2 and 3), Lavoie and al. (2016) and Bordeleau et al. (2017) also found geochemical and physical evidence of upward flow near the Jacques Cartier River Fault, suggesting that it could act as a preferential pathway to brine migration.

While the numerical model presented in the previous Section does indicate the presence of a regional flow system reaching substantial depths and emerging near the St. Lawrence River, interactions between this regional flow system and the Jacques Cartier River fault zone, remains to be understood.

In this Section, the potential role of a fault zone in a regional groundwater discharge area will thus be investigated through further numerical simulations. Since some data gaps exist in the physical characterization of the deep subsurface in the study area, this analysis does not attempt to deliver a definitive interpretation of the flow dynamics occurring near the Jacques-Cartier River Fault. The intent is rather to explore what impact different fault configurations would have on the hydraulic gradients and the distribution of mean groundwater ages near the fault zone as a basis for further studies.

3.5.1 Modeled fault configurations

In the context of this study, the fault zone is considered to be the volume of rock where the permeability has been altered as a result of fault-related deformations, while the protolith is considered the undeformed rock surrounding the fault zone (Bense et al. 2013). Resulting from tectonic activity, fault zones are complex hydraulic structures with various degrees of deformation. The fault core (FC) generally refers to the central zone of the fault which has undergone the most intense strain and most of the displacement and as result can have a lower permeability than the protolith (Bense et al. 2013). On the other hand, the damage zone (DZ), surrounding the fault core, is defined as the region which absorbed the remaining strain and as a result is marked by fracturing and an enhanced permeability (Bense et al. 2013).

The degree and nature of the rock deformation attributed to faulting depends many intrinsic controls such as lithology, fault displacement and geometry, and deformation conditions (Caine et al. 1996) which are complex to characterize. Furthermore, the definition of the fault's permeability structure has also been shown to depend on the observation methods and geoscience discipline (Scibek et al. 2016).

Larger scale fault structures are often segmented and complex, exhibiting multiple fault cores and overlapping damage zones (Bense et al. 2013). In the current study, for the sake

of simplicity and based on the conceptual model of Ladevèze (2017), the Jacques-Cartier River fault zone permeability structure is represented by the simplified conduit-barrier-conduit model (Figure 39). In this model the fault core is less permeable and the damage zone more permeable than the protolith.

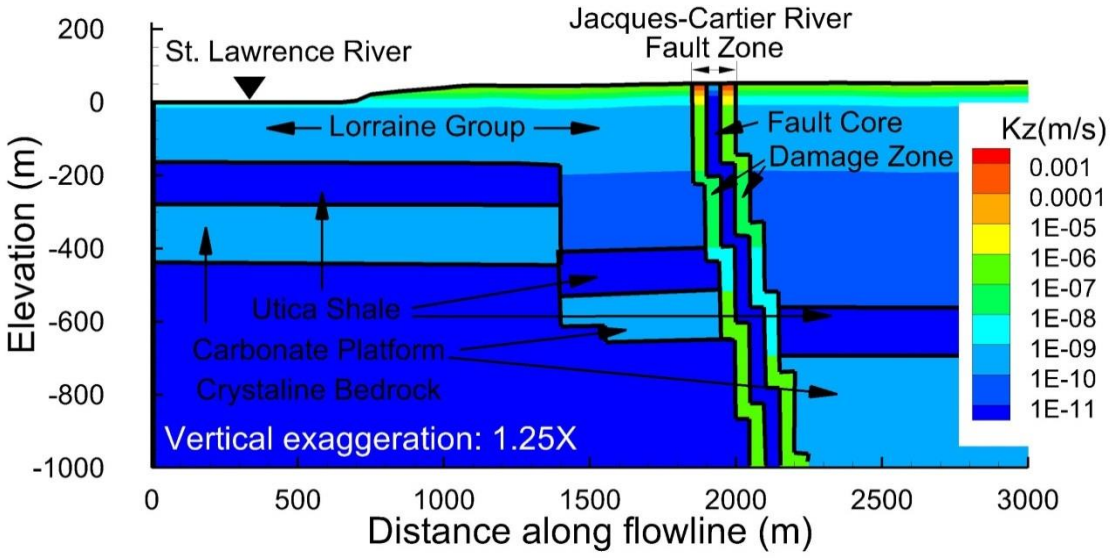

Figure 38 Jacques-Cartier River fault zone conceptual model. Vertical hydraulic conductivities shown correspond to scenario P of the parametric study on faults.

A number of fault characteristics such as the dip, the thickness and permeabilities of the fault zone and those of its core and its damage zone can play a role in controlling the fluid flow around a fault (Bense et al. 2013). This study will focus on the impact of the permeability contrasts between the different fault zones by simulating a range of fault permeability structures (Table 8). Since the scale and nature of the hydrogeological numerical model herein is not suited for representing discrete fractures, the damage zone and fault core are represented through equivalent porous media. The geometry and dip of the fault are based on the geologic cross-Section of Séjourné et al. (2013) (Figures 3 and 38) extending from the bedrock surface to the top of the crystalline Grenville formation. The thickness of the modeled fault core and the two damage zones corresponds to the width of one element (50 m). For the different scenarios, the horizontal and vertical hydraulic conductivities of the fault core and damage zones are increased or decreased by 1-3 orders of magnitude with respect to the laterally adjacent elements corresponding to the protolith

(Table 8), while retaining their original anisotropy. As the hydraulic conductivity of the Lorraine Group decreases with depth so does that of the fault zone when it crosses the Lorraine Group. For comparison, tested scenarios also include conduit-only and barrier-only fault types.

Table 8 Simulated fault permeability scenarios

Scenario	Fault Core (FC) hydraulic conductivity contrast with protolith (P) in x and z directions	Damage Zone (DZ) hydraulic conductivity contrast with protolith (P) in x and z directions	Permeability Conceptual Model
A	$K_{FC} = K_P$	$K_{DZ} = K_P$	Base Case
B	$K_{FC} = K_P \times 0.1$	$K_{DZ} = K_P$	Barrier
C	$K_{FC} = K_P \times 0.01$	$K_{DZ} = K_P$	Barrier
D	$K_{FC} = K_P \times 0.001$	$K_{DZ} = K_P$	Barrier
E	$K_{FC} = K_P$	$K_{DZ} = K_P \times 0.1$	Conduit
F	$K_{FC} = K_P \times 0.1$	$K_{DZ} = K_P \times 0.1$	Conduit-Barrier-Conduit
G	$K_{FC} = K_P \times 0.01$	$K_{DZ} = K_P \times 0.1$	Conduit-Barrier-Conduit
H	$K_{FC} = K_P \times 0.001$	$K_{DZ} = K_P \times 0.1$	Conduit-Barrier-Conduit
I	$K_{FC} = K_P$	$K_{DZ} = K_P \times 0.01$	Conduit
J	$K_{FC} = K_P \times 0.1$	$K_{DZ} = K_P \times 0.01$	Conduit-Barrier-Conduit
K	$K_{FC} = K_P \times 0.01$	$K_{DZ} = K_P \times 0.01$	Conduit-Barrier-Conduit
L	$K_{FC} = K_P \times 0.001$	$K_{DZ} = K_P \times 0.01$	Conduit-Barrier-Conduit
M	$K_{FC} = K_P$	$K_{DZ} = K_P \times 0.001$	Conduit
N	$K_{FC} = K_P \times 0.1$	$K_{DZ} = K_P \times 0.001$	Conduit-Barrier-Conduit
O	$K_{FC} = K_P \times 0.01$	$K_{DZ} = K_P \times 0.001$	Conduit-Barrier-Conduit
P	$K_{FC} = K_P \times 0.001$	$K_{DZ} = K_P \times 0.001$	Conduit-Barrier-Conduit

3.5.2 Results: groundwater flow and age

Flow and age transport results for the various fault scenarios (Annex C, Figures C1 to C4) show that in the simulated flow system a hydraulic conductivity contrast of at least two orders of magnitude between the protolith and the fault zone is required to observe significant diversion of the regional flow system. If the fault is acting as a barrier only, effects of the fault on the flow system begin to be observable when the fault zone hydraulic conductivity is two orders of magnitude less than that of the protolith but becomes truly significant with a three order of magnitude difference. Conversely, when the fault is acting as a conduit only, flow diversion is observable with only one order of magnitude difference in hydraulic conductivities between the fault and the protolith and, with a two order magnitude difference, the conduit behaviour of the fault becomes clearly evident. This

indicates that in the simulated system, the higher K of the damage zone exerts a greater influence on the flow system than the low K fault core (Annex C, Figure C2).

From an age transport perspective (Annex C, Figures C3 and C4), the presence of an effective barrier, that is a fault core with a hydraulic conductivity of at least 3 orders of magnitude lower than that of the protolith, has the effect of lowering the active flow interface and decreasing the mean ground water ages downstream of the fault (Annex C, Figure C4-D). By blocking regional flow, the barrier fault isolates the downstream flow system and local flow can penetrate deeper. Interestingly, an effective conduit-type fault, with a hydraulic conductivity at least two orders of magnitude higher that the protolith, has a dual effect on the distribution of mean groundwater ages. For the regional flow system, the conduit-type fault zone is an effective preferential pathway, through which old water from regional flow is concentrated which may reach the surface (Annex C, Figures C4-I C4-M). However, in terms of the local flow system, the conduit-type fault also somewhat behaves as a drain, drawing water into the fault zone and thereby decreasing the mean groundwater ages and lowering the active flow interface upstream of the fault. This has the effect of displacing the old water plume from upstream to downstream of the fault (Annex C, Figures C4-I C4-M).

Combining a barrier type fault core flanked with a conduit -type damage zone emphasizes the effects of both the barrier and conduit zones (Annex C, Figure C4-P). On the upstream side of the fault zone, the damage zone channels regional flow which is then effectively blocked by the fault core, allowing the plume of older water to reach closer to the surface before mixing with the local system. On the downstream side of the fault, the damage zone acts a channel for local flow, allowing recharge to penetrate deeper into the subsurface and creating a larger mixing zone.

The most important outcome from this parametric study is that in the regional discharge area, the presence of a fault with a damage zone and/or fault core with a significantly contrasting hydraulic conductivity with the protolith has the potential to divert and channel regional flow similar to a preferential pathway.

Nonetheless, this study represents a simplified model of the Jacques-Cartier fault and should only be viewed as a basis for further fault zone characterizations. To more accurately assess the impact of the Jacques-Cartier fault on the emergence of regional flow and its potential to act a contamination pathway related to fracking activities, further modelling should be performed taking into account the full complexity of fault zone hydrogeology. Such a model should refine the definition of the permeability structure of the fault zone and consider additional hydrodynamic processes which are relevant to deep basin flow such as density-dependent flow, pressure gradients in deep formations and multiphase flow.

4. Discussion

The aim of this study was to reinforce understanding of regional flow dynamics in the Chaudière-Appalaches region through the analysis of characteristic time scales using geochemistry and numerical modelling. The conceptual model, presented in Section 2.4, is based on Tóth's (1999) topography-driven flow model and outlines the presence of local, intermediate and regional-scale flow systems.

The main regional aquifer was reported to be located in the fractured bedrock (Lefebvre et al. 2015; Benoît et al. 2014; Brun Koné 2013) and the numerical modelling presented herein confirms that the logarithmically decreasing hydraulic conductivity of the bedrock maintains the active flow of groundwater in the top 40 m of the fracture rock. While simulated mean groundwater ages in the active flow zones are less than a 100 years, advective travel times in the local flow systems can reach up to approximately 0.65 Ma and mean groundwater ages up to more than 1 Ma. The slightly shallower active and local flow systems in the St. Lawrence Lowlands with respect to the Appalachian Highlands, highlights the effect of topographic relief on the local flow systems.

Rapid increases of travel times and mean groundwater ages with depth in the local flow system appears to match the conceptual geochemical distribution model of the different water types in the study region. As explored in Section 2.3, from the analysis of groundwater samples taken from residential wells, three major water types prevail in the study area. First, G1 samples, with typical recharge water geochemical signatures (Ca-HCO_3) are found both in the St. Lawrence Lowlands and the Appalachian Highlands. Most of the samples of this water type were identified as being in an open system with respect to the atmosphere and those in a closed system have the lowest radiocarbon ages found among the three water types. G1 water mostly corresponds to the active flow layer of the simulated system where the rate of flow is the fastest. Residential wells, however, extend on average to a depth of 60 m, at which point, according to our simulations, water would also be drawn from below the active flow zone yielding a maximum radiocarbon age of 3500 yrs B.P. in this water group. Furthermore, local flow systems in the study area can extend to a depth of approximately 200 m, can have advective travel times reaching up to approximately 0.65 Ma, and are likely affected by the vertical upward diffusion of old water from the regional

flow system. Therefore a water composition gradient is expected to occur within a same local flow system.

Moreover, in the model, the depth of 60 meters also roughly matches the zone where mean groundwater ages correspond to the retreat of the Champlain Sea. In the St. Lawrence Lowlands, above the mean groundwater age threshold of 10,000 years, approximately 60 m below the surface, the salty water that infiltrated the aquifers during the Champlain Sea invasion episode has been replaced by fresh recharge at least once. Therefore, the waters sampled above this threshold should have a geochemical signature corresponding to G1 or, if cation exchange sites with Na+ ions are present, to G2 (Na-HCO_3) water which corresponds to the first step of the freshening process. Recall that the presence of G2-type waters indicates that salty water which infiltrated the aquifer has been replaced by fresh water.

Water drawn from residential wells below the 10,000 year threshold will most likely be a mixture of salty water from the invasion episode and water that has recharged within the local flow system before the invasion. Given the relatively shallow nature of local flow systems, it would also be highly probable for a residential well to intercept an intermediate or even the regional flow system. Residential wells, however, are often installed as open boreholes in the bedrock and thus the water they yield is a mixture of the different geochemical layers they cross. As shown by the numerical flow model, flow volume decreases drastically with depth, thus contributions from the deeper layers of local flow systems and those of the regional system are expected to be less significant than those of the active flow layer. Nevertheless, the occurrence of G3 water samples (Na-HCO_3/Na-Cl), with a maximum radiocarbon age of 11,680 yrs B.P., validates the hypothesis that some wells extend to older water horizons. G3 water types were identified as resulting from either stagnation zones, long travel paths or mixing with older waters such as formation brines. The work of Vautour et al. (2015), Saby et al. (2016) and Bordeleau et al. (2017) also emphasizes the presence of old recharge water and connate brines in near -surface groundwater samples collected in the St. Lawrence Platform.

Bordeleau et al. (2017) collected two water samples in the Saint-Édouard-de-Lotbinière area, near the northern end of the modelled cross-Section, at a depth of 48 m below the

surface without disturbing the water column in the well and dated the samples over 1.5 Ma, further adding to the validity of our numerical groundwater model.

The samples analysed by Bordeleau et al. (2017) were collected near regional fault lines suggesting regional faults such as the Jacques-Cartier River fault could act as preferential discharge pathways to regional flow. The parametric study on fault zone permeability distributions showed that several orders of magnitude difference in hydraulic conductivities between the protolith, the damage zone and the fault core is required for the conduit/barrier effect of the fault to be significant. However, the study also demonstrated that fault zones can indeed concentrate the input of regional flow to the active flow zone. Regional flow in the Chaudière-Appalaches is almost insignificant with respect to the active flow system and its occurrence is therefore difficult to observe in the field. However, large-scale heterogeneities such as faults which have the effect of concentrating flow, can enhance the detectability of regional flow in near-surface groundwater samples.